RETINAL VESSEL DETECTION IN WIDE-FIELD FLUORESCEIN ANGIOGRAPHY WITH DEEP NEURAL NETWORKS: A NOVEL TRAINING DATA GENERATION APPROACH

Li Ding[1]*, Ajay Kuriyan*[2]*, Rajeev Ramchandran*[2]*, and Gaurav Sharma*[1]

[1]Dept. of Electrical and Computer Engineering, [2]Dept. of Ophthalmology,
University of Rochester, Rochester, NY

ABSTRACT

Retinal blood vessel detection is a crucial step in automatic retinal image analysis. Recently, deep neural networks have significantly advanced the state of the art for retinal blood vessel detection in color fundus (CF) images. Thus far, similar gains have not been seen in fluorescein angiography (FA) because the FA modality is entirely different from CF and annotated training data has not been available for FA imagery. We address retinal vessel detection in wide-field FA images with generative adversarial networks (GAN) via a novel approach for generating training data. Using a publicly available dataset that contains concurrently acquired pairs of CF and fundus FA images, vessel maps are detected in CF images via a pre-trained neural network and registered with fundus FA images via parametric chamfer matching to a preliminary FA vessel detection map. The co-aligned pairs of vessel maps (detected from CF images) and fundus FA images are used as ground truth labeled data for de novo training of a deep neural network for FA vessel detection. Specifically, we utilize adversarial learning to train a GAN where the generator learns to map FA images to binary vessel maps and the discriminator attempts to distinguish generated vs. ground-truth vessel maps. We highlight several important considerations for the proposed data generation methodology. The proposed method is validated on VAMPIRE dataset that contains high-resolution wide-field FA images and manual annotation of vessel segments. Experimental results demonstrate that the proposed method achieves an estimated ROC AUC of 0.9758.

Index Terms— Fluorescein angiography, vessel detection, generative adversarial networks, deep learning, retinal image analysis

1. INTRODUCTION

Fluorescein angiography (FA) is an established method to visualize, assess, and understand the impact of retinal disorders. It involves an intravenous injection of fluorescein dye and images are recorded as the dye courses through the vasculature. The image acquisition utilizes either a scanning laser ophthalmoscope, which produces wide-field FA images, or a digital fundus camera for capturing fundus FA images. The latter is also commonly used for capturing color fundus (CF) images. Compared to fundus FA images or CF images, the wide-field FA images have distinct advantage that they provide a wide field of view (FOV). Typically, CF images capture only a 30° to 60° FOV whereas wide-field FA allows a 200° FOV that covers about 82% surface of retina. The wide FOV allows imaging of retinal periphery, which makes it possible to measure the relative changes in peripheral retinal vessels.

In current clinical settings, wide-field FA images are manually examined by ophthalmologists to assess changes and abnormalities in retinal vessels. Because of limited time during clinical visits, such assessments are normally qualitative. Quantitative manual analysis of wide-field FA images, although are highly desirable, are extremely time-consuming process and are impractical in clinical practice. This motivates the computer-assisted retinal image analysis that provides quantitative assessments to correlate with disease and treatment progression. To this end, accurate vessel detection in wide-field FA images is a crucial step that makes reliable measurements of vasculature changes possible.

Deep learning methodologies have recently led to compelling improvements in performance for a variety of computer vision tasks [1–3], including retinal image analysis from CF imagery [4, 5], which is the predominant form of retinal imagery. Highly accurate vessel detection in CF images has been demonstrated using Convolutional Neural Networks (CNNs) [6–8], enabled by reasonably sized ground truth labeled datasets [9–12] used in combination with data augmentation techniques. Specifically, most techniques make use of the DRIVE [11] and STARE [12] datasets that provide 40 and 20 color fundus images along with corresponding vessels maps, respectively. The current state of the art is represented by [13] where an adversarial learning approach is adopted that utilizes an additional discriminator network to reduce false positive detections.

While trained deep neural networks are very successful in detecting vessels in CF images, these same networks cannot be used for wide-field FA images because the imaging modalities are vastly different. The deployment of deep networks for vessel detection for wide-field FA imagery has been stymied by the absence of labeled ground truth datasets. Unfortunately, only one dataset is publicly available for wide-field FA images, i.e., the VAMPIRE dataset [14] that contains 8 high resolution wide-field images with manual annotation of ground truth vessel maps.

Manually labeling vessels is tedious and expensive. In this paper, we propose a method for vessel detection in FA images with deep neural network via a novel approach for generating training data. The training data generation is motivated by the availability of a dataset that consists of concurrently acquired CF images and fundus FA images [15]. We apply pre-trained neural networks to accurately detect blood vessels in CF images, which are further registered with fundus FA images via parametric chamfer alignment to a preliminary vessel map obtained with a pre-existing technique. The co-aligned pairs of fundus FA images and vessel maps are then used to train a generative adversarial network for vessel detection in wide-field FA images.

The proposed method has several advantages. First, the generation of training data from CF images and fundus FA images is appealing because it eliminates tedious and time-consuming manual annotation. Second, wide-field FA images normally exhibit variation in image contrast, especially in peripheral regions that have low intensity and contrast. Contrast and exposure poses a big challenge for manual and automated annotation. The proposed cross-modality approach, however, builds in invariance to contrast and exposure. The use of parametric chamfer alignment for our registration procedure is also well-matched and advantageous in the proposed automated approach for training data generation for two reasons. Firstly, finding

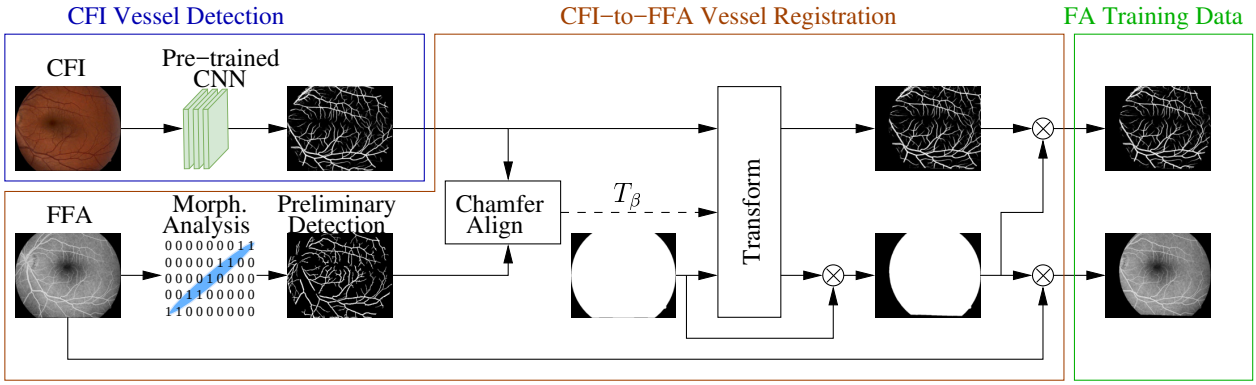

Fig. 1. Overview of the proposed approach for generating training data. CFI: color fundus images; FFA: fundus fluorescein angiography. In the first block (blue), the vessel maps in CF images are detected using pre-trained neural networks. In the second block (brown), vascular networks are registered via chamfer alignment. The overlapping area between CFI and FFA is also estimated. The inferred training data, as shown in the last block (green), includes FFA and co-aligned vessel maps that remains in the overlapping area. Best viewed in color.

matching feature points is quite challenging for the vastly different CF and FA modalities and by using parametric chamfer alignment, we eliminate this challenge. Second, the asymmetric nature of the chamfer alignment formulation allows us to obtain a precise alignment using a preliminary vessel detection with a low false positive rate, even if the corresponding true positive rate is also low.

While the imaging systems for fundus FA images and wide-field FA images are different, they both rely on the same underlying modality (fluorescein angiography) and therefore share common characteristics in the captured imagery. This allows a deep neural network that is trained on fundus FA images to detect retinal blood vessels from wide-field FA images.

The paper is organized as follows. Section 2 describes the novel approach for generating training data, which is used to train a GAN in Section 3. We present the experimental results in Section 4, and summarize concluding remarks in Section 5.

2. TRAINING DATA GENERATION FOR FA IMAGERY

In this section, we describe the proposed novel approach to create a training dataset, which is motivated by the availability of a publicly available database of CF images and corresponding fundus FA images [15]. Although no name was originally assigned with this database, we denote it as CFI2FFA for a concise presentation. Both images are captured at the same clinical visit but vary in capture viewpoints. For subjects free from pathology, the vessels for the two modalities should coincide. The key idea is to apply the deep neural network to extract vessels in CF images and to precisely transfer the detected vessels to fundus FA images using parametric chamfer alignment. Figure 1 shows the overview of the proposed approach.

2.1. Vessel Detection In Color Fundus Images

To detect vessels in CF images, we adopt a pre-trained deep neural network model proposed in [13] that exploits adversarial learning. The model is trained on DRIVE dataset [11] which achieves Area Under the Receiver Operating Characteristic Curve (ROC AUC) of 0.9803 and Dice Coefficient of 0.829. The pre-trained network is applied to overlapping patches of CF images in the CFI2FFA database. The final CF binary vessel map is obtained by thresholding the probability map from generator using Otsu method [16].

2.2. Vessel Registration

Preliminary vessel detection for anchoring: we adopt an unsupervised vessel detection method [17] that relies on multiple scale and orientation morphological analysis that takes into account variations in widths and directions of vessel structures. Specifically, the input FA image is decomposed into different resolutions where vessels at each scale are processed independently. A modified top-hat operator [18] with linear structuring elements with different directions is applied to detect bright and rectilinear regions in FA images. The final vessel map is achieved by fusing together the detected vessels at each scale. The vessel maps from morphological analysis are used for aligning fundus FA images with CF images.

Vessel registration with chamfer alignment: to transfer the accurate vessel segments in CF images to corresponding fundus FA images, we apply parametric chamfer alignment [19] to precisely register the pair of vessel maps. Denote the locations of vessel pixels in CF images as $\mathbf{Q} = \{\mathbf{q}_j\}_{j=1}^{N_j}$ and in fundus FA images as $\mathbf{P} = \{\mathbf{p}_i\}_{i=1}^{N_i}$, where $\mathbf{q}_j = (u_j, v_j)$ and $\mathbf{p}_i = (x_i, y_i)$. The conventional chamfer alignment is formulated as minimizing the chamfer distance $D_0(\beta)$ between the target points $\mathbf{Q}$ and the reference points $\mathbf{P}$

$$D_0(\beta) = \frac{1}{N_j} \sum_{i=j}^{N_j} \min_i \|\mathbf{p}_i - \mathcal{T}_\beta(\mathbf{q}_j)\|^2. \quad (1)$$

For each point $\mathbf{q}_j$, the nearest point in $\mathbf{P}$ is chosen to define the alignment error under the parametric transformation $\mathcal{T}_\beta$, where β is a set of parameters defining the transformation. We adopt a second-order polynomial transformation to map the target points to the reference points, which is defined as

$$\mathcal{T}_\beta(\mathbf{q}_j) = \begin{bmatrix}\beta_1 \\ \beta_7\end{bmatrix} + \begin{bmatrix}\beta_2 & \beta_3 \\ \beta_8 & \beta_9\end{bmatrix} \begin{bmatrix}u_j \\ v_j\end{bmatrix} + \begin{bmatrix}\beta_4 & \beta_5 & \beta_6 \\ \beta_{10} & \beta_{11} & \beta_{12}\end{bmatrix} \begin{bmatrix}u_j^2 \\ u_j v_j \\ v_j^2\end{bmatrix}. \quad (2)$$

The formulation in (1) is sensitive to outliers points that only exist in the target points $\mathbf{Q}$. Because of the differences in capture viewpoints, the FOV in CF image may not be coincident with that in fundus FA image. The chamfer distance of outlier points are relatively large, resulting in erroneous transformation parameters. To tackle this issue, we assign each target point $\mathbf{q}_j$ a binary latent variable χ_j, where $\chi_j = 1$ indicates the target point $\mathbf{q}_j$ is an inlier point and $\chi_j = 0$ otherwise. The conventional chamfer alignment is then

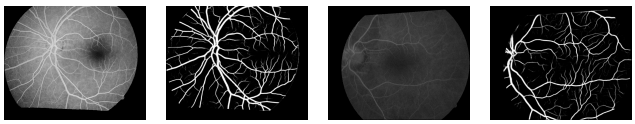

(a) (b) (c) (d)

Fig. 2. Sample results of training data generation for FA imagery. (a) and (c) show two fundus FA images, and (b) and (d) are the corresponding vessel maps. Notice that the generated vessel maps are robust under different contrast conditions.

enhanced by weighting the chamfer distance for each target point in terms of the probability that a corresponding point exists in the reference. The modified objective function is

$$D(\beta) = \frac{1}{N_j} \sum_{i=j}^{N_j} p_j \min_i \|\mathbf{p}_i - \mathcal{T}_\beta(\mathbf{q}_j)\|^2, \quad (3)$$

where p_j is the posterior probability of $\chi_j = 1$. The minimization in (3) can be viewed as a probabilistic chamfer alignment [20] and can be estimated using the expectation-maximization (EM) algorithm [21]. A detailed description can be found in [20]. Once the transformation parameters are estimated, we map the vessel maps in CF images to the corresponding fundus FA images using the estimated second-order polynomial transformation.

Parametric chamfer alignment is an advantageous tool for registration. The asymmetry of the chamfer distance allows preliminary FA vessel detector to be chosen to have high specificity despite a low sensitivity. Also, the formulation uses a global matching of the vessels instead of relying on a sparse set of feature points, which is beneficial for the polynomial parametric mapping.

To select the common region between a co-aligned image pair, we first create binary mask for original CF, which is then transformed using the estimated β. The mask for the overlapping area can be easily obtained by multiplying the transformed mask with the original one. Only pixels in the overlapping region are considered as the inferred training data.

The proposed cross-modality approach has the benefit of invariance of contrast because the inferred vessel maps are transferred from those detected in CF images. Figures 2a and 2c show two fundus FA images that have high and low contrasts, respectively. The corresponding inferred vessel maps, which are shown in Fig. 2b and 2d, provide consistent detections that capture both major and minor vessels regardless of image contrast.

3. GAN TRAINING FOR FA VESSEL DETECTION

Objective function. We exploit the recent concept of generative adversarial networks (GAN) [22] and formulate the task of vessel detection as an image-to-image translation [3]. In this context, the network includes a generator G, which is trained to learn a mapping from the FA image f to the vessel map v, and a discriminator D, which aims to distinguish between real pairs and generated pairs of fundus FA images and vessel maps. The idea is to jointly train G and D in the way that G is able to generate realistic vessel maps from f that can deceive D and that D becomes accurate at distinguishing images. The objective function for GAN is defined as

$$\mathcal{L}_{GAN} = \mathbb{E}_{f,v}[\log D(f,v)] + \mathbb{E}_f[\log(1 - D(f, G(f)))], \quad (4)$$

where the first and the second terms can be viewed as the capability that D correctly classifies the real pair (f, v) sampled from training set and the fake pair $(f, G(f))$ generated by G, respectively.

Inspired by the idea proposed in [3] that integrates a data loss ($L1$ loss) into the objective function, we combine the objective function in (4) with a conventional loss used for segmentation that penalizes the disagreement with the ground truth vessel map. The segmentation loss $\mathcal{L}_s$ is given by:

$$\mathcal{L}_s = -\mathbb{E}_{f,v}[v \log G(f) + (1 - v) \log(1 - G(f))]. \quad (5)$$

The training procedure is then a min-max game between the generator and the discriminator

$$\min_G \max_D \mathcal{L}_{GAN}(G, D) + \lambda \mathcal{L}_s(G), \quad (6)$$

where λ is the free parameter.

Network architecture. The network architecture is visualized in Fig. 3. For generator, we adopt the general idea of the U-Net [23] for the generator, which comprises a downsampling path and an upsampling path. The key component in the U-Net is the skip-connection that concatenates each upsampled feature map with the corresponding one in the downsampling path that has the same spatial resolution. The skip-connection is designed for detecting fine vessel structures. Each convolutional layer uses 3×3 kernels except for the final convolutional layer which has 1×1 kernel. The discriminator receives either an image pair $\{f, v\}$ (the blue and green bars) or $\{f, G(f)\}$ (the blue and brown bars).

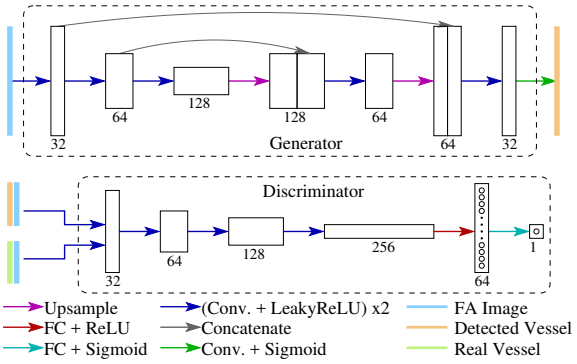

Fig. 3. Network architecture. The rectangular blocks are feature maps where heights indicate spatial dimensions. The last two blocks in the discriminator show the outputs from fully connected layers. The numbers below the rectangular block show the number of feature channels (or number of hidden units for fully connected layers). Best viewed in color.

Implementation. Compared with the network proposed in [13], which is trained on CF image dataset for vessel detection, our model differs in several ways to account for the differences between fundus FA images and wide-field FA images. To adapt to variance in image appearance, we feed the generator 256×256 patches rather than the entire image. This is motivated by the observation that the two image modalities share a similar structure locally. This strategy offers another advantage that the local contrast remains uniform over each patch. As shown in Fig. 2, the inferred training data covers a large range of contrast. With image augmentation, GAN is able to extract vessels under different contrast conditions. Because of the peripheral regions imaged, the wide-field FA images are sometimes corrupted by eyelid and eyelash shadows. To tackle this problem, we create an elliptical region of interest (ROI), which is a proper shape to cover the region of the presence of vessels because an ellipsoid mirror is used to produce the wide-field FA image. To estimate the ROI, the wide-field FA image is binarized followed by ellipse shape fitting to the largest connected component in the binary image.

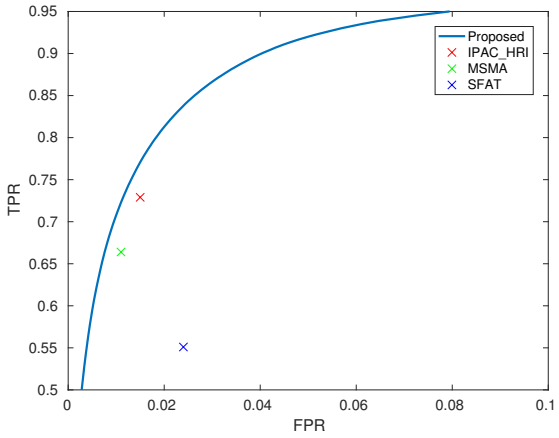

Fig. 4. ROC curve for the proposed method and the comparison with existing methods.

4. EXPERIMENTAL VALIDATION

We evaluate the proposed framework on VAMPIRE dataset [14] that consists of 8 wide-field FA images. There are two sequences in this dataset representing a healthy retina (GER) and a diseased retina (AMD). Each sequence is a time course of exposures captured progressively as the dye perfused into the vessels. The images are 3900×3072 pixels. The dataset provides ground truth binary vessel maps annotated by ophthalmologists. We compare the proposed method with several alternative approaches: SFAT [14] that is the method originally published with VAMPIRE dataset, IPAC_HRI [24] that combines infinite perimeter active contour and hybrid region information for vessel segmentation, and MSMA [17], a method based on multi-scale morphological analysis.

At the training stage, we first augment the training data by flipping and rotating the fundus FA images. Training patches are extracted from the augmented dataset. Each training patch is further augmented by randomly adjusting image brightness and contrast and by adding Gaussian noise. We use Adam optimizer [25] and stochastic gradient descent (SGD) to update G and D, respectively. The slope for LeakyReLU is 0.1. Initial learning rate is 2×10^{-4} for both G and D, which is fixed for G and is decayed with a factor of 10^{-6} for D. The free parameter λ is set to 10.

4.1. Quantitative And Qualitative Results

To quantitatively compare the performance of vessel detection, we use Receiver Operating Curve for each test image. Figure 4 plots the results of ROC curve over the 8 test images. The cross markers in Fig. 4 show results from alternative methods. The results indicate that the proposed method outperforms the existing methods on the VAMPIRE dataset. It achieves a ROC AUC of 0.9758. Figure 5 shows qualitative results for image "AMD2" in the dataset. The soft-map vessel image detected by GAN is binarized using Otsu threshold [16] to visualize true positive (green), false positive (red), false negative (blue), and true negative (black).

It is worth pointing out that the ground truth vessel maps in the VAMPIRE dataset have the issue that ophthalmologists did not label several vessel branches in low contrast regions. As mention in Section 1, contrast and exposure usually poses a big challenge for manual labeling. We illustrate this issue in Fig. 5 (see four rectangular regions highlighted in the second row). After closely examining

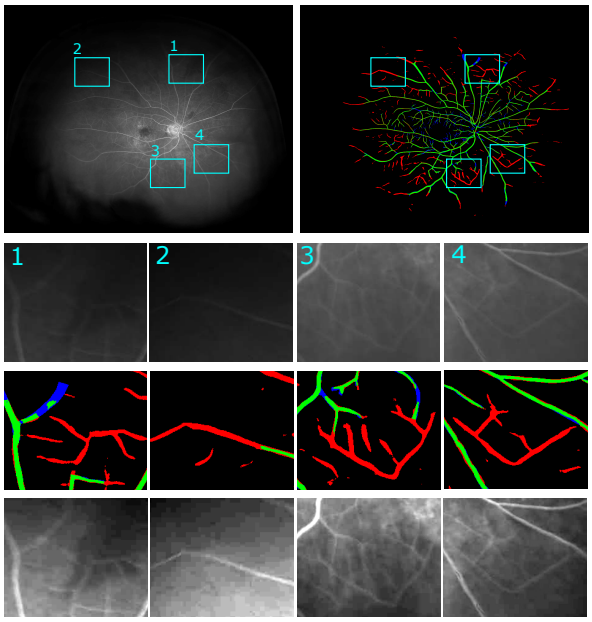

Fig. 5. Sample results of vessel detection. The first row: wide-field FA and detected vessels. Green, red, and blue indicates true positive, false positive, and false negative, respectively. The second and the third rows show the close-ups of four rectangular regions marked on the wide-filed FA images and corresponding results, respectively. The "false positive" detections are actually true vessels that are not labeled by ophthalmologists. In the last row, we show the images after contrast enhancement for a better visualization.

the vessel detection results, we observe that the "false positive" detections, which are represented by red pixels in the third row, are indeed true vessels that are not noticed by ophthalmologists. For a better visualization, we show the same regions with contrast enhancement in the last row where the missing vessels can be identify clearly. As we can see, the proposed method is much more robust to contrast variations than manual labeling.

5. CONCLUSION

In this paper, we proposed a novel approach for generating labeled ground truth data for retinal vessel detection in wide-field FA images and demonstrated the utility of the approach by training a deep generative adversarial network for the vessel detection task. Experimental validation on VAMPIRE dataset demonstrates that, both quantitatively and qualitatively, the proposed method outperforms existing methods, achieving a ROC AUC of 0.9758.

In future, the the proposed cross-modality approach for generating a training dataset for FA images is also a particularly attractive option for automatically generating larger labeled FA datasets because, in current clinical settings, baseline color fundus images are routinely captured prior to FA dye injection.

6. ACKNOWLEDGMENT

This work was supported in part by New York State Center of Excellence in Data Science award # C160189 and by a Research Award from the University of Rochester. Thanks to the Center for Integrated Research Computing, University of Rochester, for providing access to computational resources.

7. REFERENCES

[1] K. He, G. Gkioxari, P. Dollár, and R. Girshick, "Mask R-CNN," in *IEEE Intl. Conf. Comp. Vision*, 2017, pp. 2980–2988.

[2] J. Long, E. Shelhamer, and T. Darrell, "Fully convolutional networks for semantic segmentation," in *IEEE Intl. Conf. Comp. Vision, and Pattern Recog.*, 2015, pp. 3431–3440.

[3] P. Isola, J.-Y. Zhu, T. Zhou, and A. A. Efros, "Image-to-image translation with conditional adversarial networks," in *IEEE Intl. Conf. Comp. Vision, and Pattern Recog.*, July 2017.

[4] V. Gulshan, L. Peng, M. Coram, M. C. Stumpe, D. Wu, A. Narayanaswamy, S. Venugopalan, K. Widner, T. Madams, J. Cuadros *et al.*, "Development and validation of a deep learning algorithm for detection of diabetic retinopathy in retinal fundus photographs," *Jama*, vol. 316, no. 22, pp. 2402–2410, 2016.

[5] R. Poplin, A. V. Varadarajan, K. Blumer, Y. Liu, M. V. McConnell, G. S. Corrado, L. Peng, and D. R. Webster, "Predicting cardiovascular risk factors from retinal fundus photographs using deep learning," *arXiv preprint arXiv:1708.09843*, 2017.

[6] K.-K. Maninis, J. Pont-Tuset, P. Arbeláez, and L. Van Gool, "Deep retinal image understanding," in *Intl. Conf. Med. Image Computing and Computer-Assisted Intervention*, 2016, pp. 140–148.

[7] P. Liskowski and K. Krawiec, "Segmenting retinal blood vessels with deep neural networks," *IEEE Trans. Med. Imaging*, vol. 35, no. 11, pp. 2369–2380, Nov 2016. doi: 10.1109/TMI.2016.2546227

[8] H. Fu, Y. Xu, S. Lin, D. W. K. Wong, and J. Liu, "Deepvessel: Retinal vessel segmentation via deep learning and conditional random field," in *Intl. Conf. Med. Image Computing and Computer-Assisted Intervention*, 2016, pp. 132–139.

[9] A. Budai, R. Bock, A. Maier, J. Hornegger, and G. Michelson, "Robust vessel segmentation in fundus images," *Intl. J. Biomedical Imaging*, vol. 2013, 2013.

[10] E. Decencière, X. Zhang, G. Cazuguel, B. Lay, B. Cochener, C. Trone, P. Gain, R. Ordonez, P. Massin, A. Erginay *et al.*, "Feedback on a publicly distributed image database: the Messidor database," *Image Analysis & Stereology*, vol. 33, no. 3, pp. 231–234, 2014.

[11] J. Staal, M. Abramoff, M. Niemeijer, M. Viergever, and B. van Ginneken, "Ridge based vessel segmentation in color images of the retina," *IEEE Trans. Med. Imaging*, vol. 23, no. 4, pp. 501–509, 2004.

[12] A. Hoover, V. Kouznetsova, and M. Goldbaum, "Locating blood vessels in retinal images by piecewise threshold probing of a matched filter response," *IEEE Trans. Med. Imaging*, vol. 19, no. 3, pp. 203–210, 2000.

[13] J. Son, S. J. Park, and K.-H. Jung, "Retinal vessel segmentation in fundoscopic images with generative adversarial networks," *arXiv:1706.09318*, 2017.

[14] A. Perez-Rovira, K. Zutis, J. Hubschman, and E. Trucco, "Improving vessel segmentation in ultra-wide field-of-view retinal fluorescein angiograms," in *IEEE Intl. Conf. Eng. in Med. and Biol. Soc.*, 2011, pp. 2614–2617.

[15] S. Hajeb Mohammad Alipour, H. Rabbani, and M. R. Akhlaghi, "Diabetic retinopathy grading by digital curvelet transform," *Comput. and Math. Methods in Med.*, vol. 2012, 2012.

[16] N. Otsu, "A threshold selection method from gray-level histograms," *IEEE Intl. Conf. Systems, Man and Cyber.*, vol. 9, no. 1, pp. 62–66, 1979.

[17] L. Ding, A. Kuriyan, R. Ramchandran, and G. Sharma, "Multi-scale morphological analysis for retinal vessel detection in wide-field fluorescein angiography," in *Proc. IEEE Western NY Image and Signal Proc. Wksp.*, 2017. doi: 10.1109/WNYIPW.2017.8356256 pp. 1–5.

[18] A. M. Mendonca and A. Campilho, "Segmentation of retinal blood vessels by combining the detection of centerlines and morphological reconstruction," *IEEE Trans. Med. Imaging*, vol. 25, no. 9, pp. 1200–1213, Sept 2006. doi: 10.1109/TMI.2006.879955

[19] L. Ding, A. Kuriyan, R. Ramchandran, and G. Sharma, "Quantification of longitudinal changes in retinal vasculature from wide-field fluorescein angiography via a novel registartion and change detection approach," in *IEEE Intl. Conf. Acoust., Speech, and Signal Proc.*, 2018, pp. 1070–1074.

[20] A. Elliethy and G. Sharma, "Automatic registration of wide area motion imagery to vector road maps by exploiting vehicle detections," *IEEE Trans. Image Proc.*, vol. 25, no. 11, pp. 5304–5315, Nov. 2016. doi: 10.1109/TIP.2016.2601265

[21] A. P. Dempster, N. M. Laird, and D. B. Rubin, "Maximum likelihood from incomplete data via the EM algorithm," *J. Roy. Statist. Soc. B (methodol.)*, pp. 1–38, 1977.

[22] I. Goodfellow, J. Pouget-Abadie, M. Mirza, B. Xu, D. Warde-Farley, S. Ozair, A. Courville, and Y. Bengio, "Generative adversarial nets," in *Adv. in Neural Info. Proc. Sys.*, 2014, pp. 2672–2680.

[23] O. Ronneberger, P. Fischer, and T. Brox, "U-net: Convolutional networks for biomedical image segmentation," in *Intl. Conf. Med. Image Computing and Computer-assisted Intervention*. Springer, 2015, pp. 234–241.

[24] Y. Zhao, L. Rada, K. Chen, S. P. Harding, and Y. Zheng, "Automated vessel segmentation using infinite perimeter active contour model with hybrid region information with application to retinal images," *IEEE Trans. Med. Imaging*, vol. 34, no. 9, pp. 1797–1807, 2015.

[25] D. P. Kingma and J. Ba, "Adam: A method for stochastic optimization," in *Intl. Conf. Learning Representations*, 2015.